Developmental Cell
Article

A Genome-Wide Screen Reveals a Role for microRNA-1 in Modulating Cardiac Cell Polarity

Isabelle N. King,[1,2,3,6,*] Li Qian,[1,2,6] Jianping Liang,[2] Yu Huang,[1,2] Joseph T.C. Shieh,[1,2,4] Chulan Kwon,[1,5] and Deepak Srivastava[1,2,*]
[1]Gladstone Institute of Cardiovascular Disease, San Francisco, CA 94158, USA
[2]Department of Pediatrics
[3]Division of Critical Care
[4]Division of Medical Genetics
University of California San Francisco, San Francisco, CA 94143, USA
[5]Division of Cardiology, Johns Hopkins University School of Medicine, Baltimore, MD 21205, USA
[6]These authors contributed equally to the work
*Correspondence: iking@gladstone.ucsf.edu (I.N.K.), dsrivastava@gladstone.ucsf.edu (D.S.)
DOI 10.1016/j.devcel.2011.03.010

SUMMARY

Many molecular pathways involved in heart disease have their roots in evolutionarily ancient developmental programs that depend critically on gene dosage and timing. MicroRNAs (miRNAs) modulate gene dosage posttranscriptionally, and among these, the muscle-specific *miR-1* is particularly important for developing and maintaining somatic/skeletal and cardiac muscle. To identify pathways regulated by *miR-1*, we performed a forward genetic screen in *Drosophila* using wing-vein patterning as a biological assay. We identified several unexpected genes that genetically interacted with *dmiR-1*, one of which was *kayak*, encodes a developmentally regulated transcription factor. Additional studies directed at this genetic relationship revealed a previously unappreciated function of *dmiR-1* in regulating the polarity of cardiac progenitor cells. The mammalian ortholog of *kayak*, *c-Fos*, was dysregulated in hearts of gain- or loss-of-function *miR-1* mutant mice in a stress-dependent manner. These findings illustrate the power of *Drosophila*-based screens to find points of intersection between miRNAs and conserved pathways in mammals.

INTRODUCTION

microRNAs (miRNAs) are small noncoding RNA species that regulate mRNA translation or stability and, thereby, protein dosage in eukaryotes (for review, see Inui et al., 2010). miRNAs interact with their target RNAs primarily through complementary base pairing to the 3′ UTRs of the target gene mRNAs. This Watson-Crick pairing, generally involving the 5′ region of the miRNA, results in RNA degradation and/or inhibition of translation (for review, see Bartel, 2009). Deletion of *Dicer*, the endonuclease necessary to form miRNAs, results in lethality during gastrulation, implying that miRNAs are necessary for the formation of the body plan (Bernstein et al., 2003). Specific miRNAs play critical roles in myriad processes, including cell fate, cellular differentiation, cancer, apoptosis, and stress responses (for review, see Croce, 2009; Cordes and Srivastava, 2009; Mendell, 2005; Williams et al., 2009). In most cases, the regulatory function of individual miRNAs is achieved by control of multiple steps within a common pathway. Despite significant progress, the physiologic function of and pathways regulated by most miRNAs remain unknown.

miR-1 is one of the most evolutionarily conserved miRNAs and is highly enriched in heart and muscle. In vertebrates, two distinct loci for the *miR-1/miR-133* cluster, likely a result of gene duplication, encode identical mature *miR-1*s derived from each locus (i.e., *miR-1-1* and *miR-1-2*). Loss of the single *dmiR-1* in *Drosophila* results in cardiac-specification defects in a subset of flies (Kwon et al., 2005) and catastrophic failure of somatic muscle development during the second instar stage (Sokol and Ambros, 2005). In mice, loss of *miR-1-2* results in a broad range of abnormalities, including ventricular septal defects, defects in cell-cycle control, and disturbed electrophysiological properties (Zhao et al., 2005, 2007).

Using a combination of bioinformatic and biochemical approaches, we and others have found transcription factors (Zhao et al., 2005, 2007; Ikeda et al., 2009), receptor ligands (Kwon et al., 2005; Ivey et al., 2008), ion channels (Yang et al., 2007), antiapoptotic proteins (Xu et al., 2007), and modifiers of histone acetylation (Chen et al., 2006) that are directly responsive to *miR-1* regulation. However, the number of genes known to directly respond to *miR-1* or other miRNAs is only a small fraction of the total number of miRNA-sensitive genes and pathways. Therefore, an experimental method to discover pathways regulated by specific miRNAs in vivo would be useful. Uncovering the points of intersection between a particular miRNA and basic cellular processes would allow for a more comprehensive understanding of the miRNA's function within the context of an intact cell or organ system.

Here, we describe a genome-wide enhancer/suppressor screen using the power of *Drosophila* genetics to identify cellular pathways regulated by *miR-1*. We discovered an interaction of

miR-1 with numerous factors, including the transcription factor kayak, revealing an unexpected function for *dmiR-1* in controlling cell polarity of cardiac progenitors during development. The mammalian ortholog of *kayak*, *c-Fos*, was also dysregulated upon manipulation of *miR-1* levels in the mouse heart, highlighting the utility of *Drosophila*-based assays for studying miRNA-dependent pathways in mammals.

RESULTS

Genome-Wide Enhancer/Suppressor Screen for Genetic Interaction with *miR-1*

Many of the signals that determine body axis formation and cell fate are operational in the *Drosophila melanogaster* wing and are evolutionarily conserved between widely divergent species and tissues. Because the fly wing is easy to visualize and is a nonessential organ, it is often used for high-throughput genetic screening. The morphogen *decapentaplegic* (*dpp*) is normally expressed in the wing imaginal disc, the precursor of the adult fly wing structure, between the long veins number three and four (L3, L4). We generated a fly line that contains the *dpp* promoter driving GAL4 (*dpp*-GAL4) (Bloomington Stock Center) and a GAL4-sensitive upstream activating sequence (*UAS*) regulating a *dmiR-1* transgene (*UAS-dmiR-1*) on the third chromosome. These mutant animals were viable to adulthood and were fertile, but exhibited a loss of wing tissue between veins L3 and L4, creating a scorable phenotype (Figure 1A).

We hypothesized that genetic partners of *dmiR-1* could be identified by scoring the wings for loss or gain of intervein distance (''enhancement'' or ''suppression'' of the wing phenotype, respectively). The wing phenotype was sensitive to temperature; higher temperatures (22°C–25°C) resulted in higher transcriptional activity of *GAL4* and more severe loss of wing tissue between L3 and L4 (data not shown). Due to this temperature sensitivity, all assays involving the *dpp-GAL4::UAS-dmiR-1* flies were performed at 18°C. The loss of tissue did not appear to be the result of deranged cell size, as the spacing of the hairs, which serves as a crude marker for cell size (Garcia-Bellido et al., 1994), was not significantly changed. Control crosses on wild-type backgrounds revealed rates of enhancement or suppression of the wing-vein phenotype among offspring of 8% or 3%, respectively (Figure 1A).

To identify genes that interact genetically with *dmiR-1*, the *dpp-GAL4::UAS-dmiR-1* fly line was crossed with chromosome deficiency lines obtained from DrosDel (Ryder et al., 2007; Cambridge, UK) and Bloomington Stock Center (Bloomington, IN). Each line within these deficiency kits contains a molecularly defined heterozygous deletion within one of the four *Drosophila* chromosomes. From 284 deficiency matings (representing approximately 70% of the fly genome), 32 fly lines (11%) had enhanced loss of wing tissue between L3 and L4 in at least 50% of offspring, while 252 lines (89%) had no effect on the *dmiR-1*-mediated phenotype (Figure 1B). The 32 lines that enhanced the *dmiR-1* phenotype were distributed fairly evenly among chromosomes X, 2, and 3 (Figures 1C and 1D). No progeny reproducibly rescued, or suppressed, the phenotype. Further studies were performed on the 16 fly lines harboring deficiencies on chromosome 3 (Figure 1D). Loci on chromosomes 1, 2, and 4 are the subject of ongoing studies.

To narrow the genomic regions of interest on chromosome 3, we used smaller, overlapping deficiencies. Within these deficiencies, genes implicated in transcriptional regulation, development, cell-cycle control, apoptosis, mRNA processing, *Notch* signaling, or muscle biology were given the highest ranking. If available, mutant alleles of candidate genes from chromosome 3 were requested from the Bloomington Stock Center and crossed to the *dpp-GAL4::UAS-dmiR-1* fly line. Whenever possible, multiple lines containing different mutant alleles were tested to minimize background and allele-specific effects. Mutant genes that, when heterozygous, recapitulated the enhancement of the *dpp-GAL4::UAS-dmiR-1* phenotype underwent further study.

Identification of *delta* and *mirror* Alleles Validate *dmiR-1* Enhancer Screen

In our screen, the deficiency line *Df(3R)ED5942* enhanced the *dpp-GAL4::UAS-dmiR-1* phenotype, as ~50% of progeny with the pertinent genotype had narrowing of the intervein area ($p < 0.01$). This deficiency contains the gene *delta* (*Dl*) (Figures 1D and 2A), which encodes a ligand for Notch, an important regulator of cell fate and differentiation (for review, see Bray 2006). Crosses between *dpp-GAL4::UAS-dmiR-1* flies and flies heterozygous for mutant *Dl* alleles, enhanced the *dpp-GAL4::UAS-dmiR-1* phenotype (Figures 2B and 2C; data not shown). Overexpression of wild-type *Dl* reduced the expressivity of wing vein defects in *dpp-GAL4::UAS-dmiR-1* flies in the context of a *Dl* mutant background, confirming the specificity of the genetic relationship between *Dl* and *dmiR-1* (Figures 2B and 2C, middle panels).

The deficiency lines *Df(3L)ED4486*, *Df(3L)ED4483*, and *Df(3L)BSC10* also enhanced the *dpp-GAL4::UAS-dmiR-1* phenotype (Figures 2D and 2E). Contained within these deficiency lines was the highly conserved *Iroquois* (*Iro*) gene family, which encodes homeodomain-containing transcription factors, including *mirror* (*mirr*), *araucan (ara)*, and *caupolican (caup)*. Activity of the *Iro* locus in fly is critical for establishing developmental territories within the organism (for review, see Cavodeassi et al., 2001). In mice, *Iro* family members are important for vertebrate cardiac chamber specification (Bao et al., 1999) and cardiac conduction (Costantini et al., 2005). *mirr* loss-of-function alleles greatly enhanced the *dpp-GAL4::UAS-dmiR-1* phenotype, while alleles of *ara* and *caup* displayed less robust enhancement (Figures 2E and 2F; see Figure S1 available online).

Identification of *Dl* and *mirr* mutant alleles as phenotypic enhancers validated the screen's methodology since *Dl* and *Delta-like-1* are *miR-1* targets in flies and mice, respectively (Kwon et al., 2005; Ivey et al., 2008), and *Irx5* is a target of *miR-1* in the mammalian heart (Zhao et al., 2007). Using the *Dl* and *mirr* mutants as positive controls for interpretation of affected progeny, all crosses were subsequently scored positive if ~50% of progeny (~6X above background) showed enhancement of the wing phenotype.

Identification of Genetic Partners of *dmiR-1*

The overlapping deficiencies *Df(3R)3450* and *Excel6209* enhanced the *dmiR-1* phenotype (Figures S2A and S2B; data not shown). Within these deficiencies, we identified two genes, *noa36* and *hrb98DE*, whose mutant alleles enhanced the

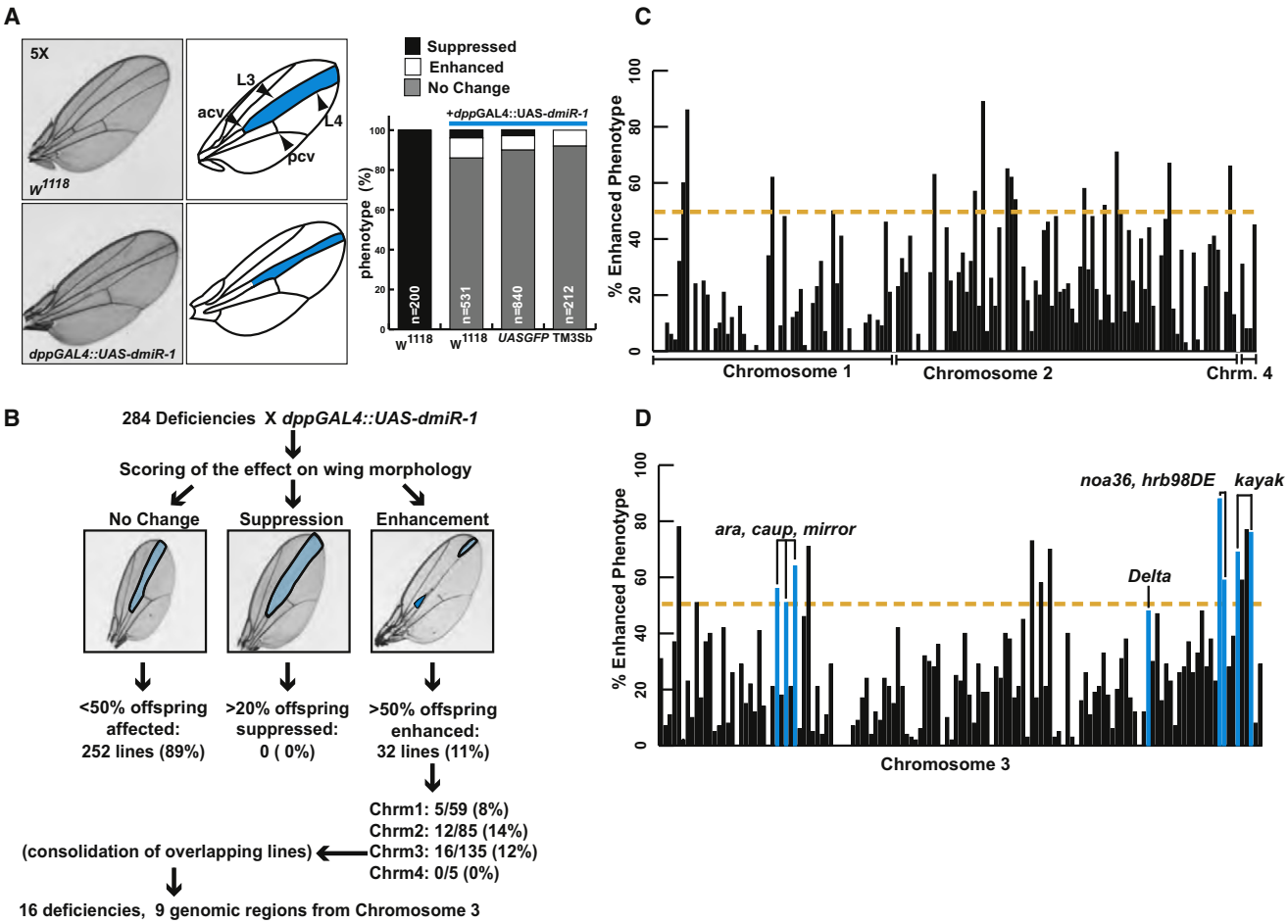

Figure 1. Misexpression of *dmiR-1* in the *Drosophila* Wing Results in a Distinctive Phenotype and Identifies Genetic Partners of *dmiR-1*

(A) Upper left: image of a wild-type wing, with pertinent anatomical structures labeled to the right. L3: long vein number 3, L4: long vein number 4, acv: anterior cross vein, pcv: posterior cross vein. Area highlighted in blue: area of expression of the wing disc specific *decapentaplegic (dpp)* enhancer. Lower left: image of wing from a *dpp-GAL4::UAS-dmiR-1* mutant fly. Note narrowing of the L3/L4 intervein distance. Right: Incidence of enhancement, and suppression of the wing phenotype seen in *dpp-GAL4::UAS-dmiR-1* mutant flies when mated with control fly lines. W^{1118}: wild-type. The lines *UAS-GFP* and *dpp-GAL4::UAS-dmiR-1/TM3Sb* (*TM3Sb*) served as controls. TM3Sb: balancer.

(B) Summary of results from the forward genetic screen.

(C) Distribution of percentage affected offspring from each deficiency, organized by chromosome (1, 2, and 4). Yellow dashed line: point at which 50% of progeny were affected. Those deficiencies that met or exceeded this level were considered strongly positive ($p < 0.0001$).

(D) Distribution of percentage affected offspring from each deficiency, organized by position on chromosome 3, going left to right. Blue bars: deficiencies containing specific genes (labeled) that enhanced the wing phenotype.

See also Table S1.

phenotype (Figures S2B and S2C and data not shown). *noa36* is predicted to bind metal ions, and *hrb98DE* acts to regulate alternative mRNA splicing. Bioinformatically, *hrb98DE* was predicted to contain four *dmiR-1* binding sites in its 3′ UTR (Stark et al., 2003) that were conserved in *Anopheles*. To determine if *dmiR-1* directly regulates *hrb98DE*, we cotransfected a *GAL4-dmiR-1* construct with a luciferase reporter construct containing 1035 bp of the 3′ UTR of *hrb98DE* into *Drosophila* Schneider 2 (S2) cells. Luciferase activity was repressed in the presence of *dmiR-1*, suggesting that *hrb98DE* was a direct target of *dmiR-1* (Figure S2D).

The deficiency lines *Df(3R)Dr-rv-1* and *Df(3R)ED6316* also enhanced the *dpp-GAL4::UAS-dmiR-1* phenotype (Figures 3A–3D). Contained within these fly deficiency lines was *kayak* (*kay*), which encodes a leucine-zipper-containing transcription factor whose mammalian ortholog is *c-Fos*. We used several different *kay* loss-of-function alleles, including a null allele ($kay^{[1]}$), a hypomorphic recessive lethal allele ($kay^{[sro-1]}$), a hypomorphic, homozygous viable allele ($kay^{[EY00283]}$), and a presumed hypomorphic allele ($kay^{[EY01644]}$). Parental lines of *kay* heterozygous mutant alleles had normal wing anatomy (Figure 3B). Mating of each of the *kay* alleles to the *dpp-GAL4::UAS-dmiR-1* fly line resulted in enhancement of the wing phenotype (Figures 3C and 3D).

To determine if the enhanced phenotype was specific to decreased *kay* function, we performed a genetic rescue assay by mating the *dpp-GAL4::UAS-dmiR-1;*$kay^{[sro-1]}$ fly to flies harboring a *UAS-kay* element (Figures 3C and 3E). Coexpression

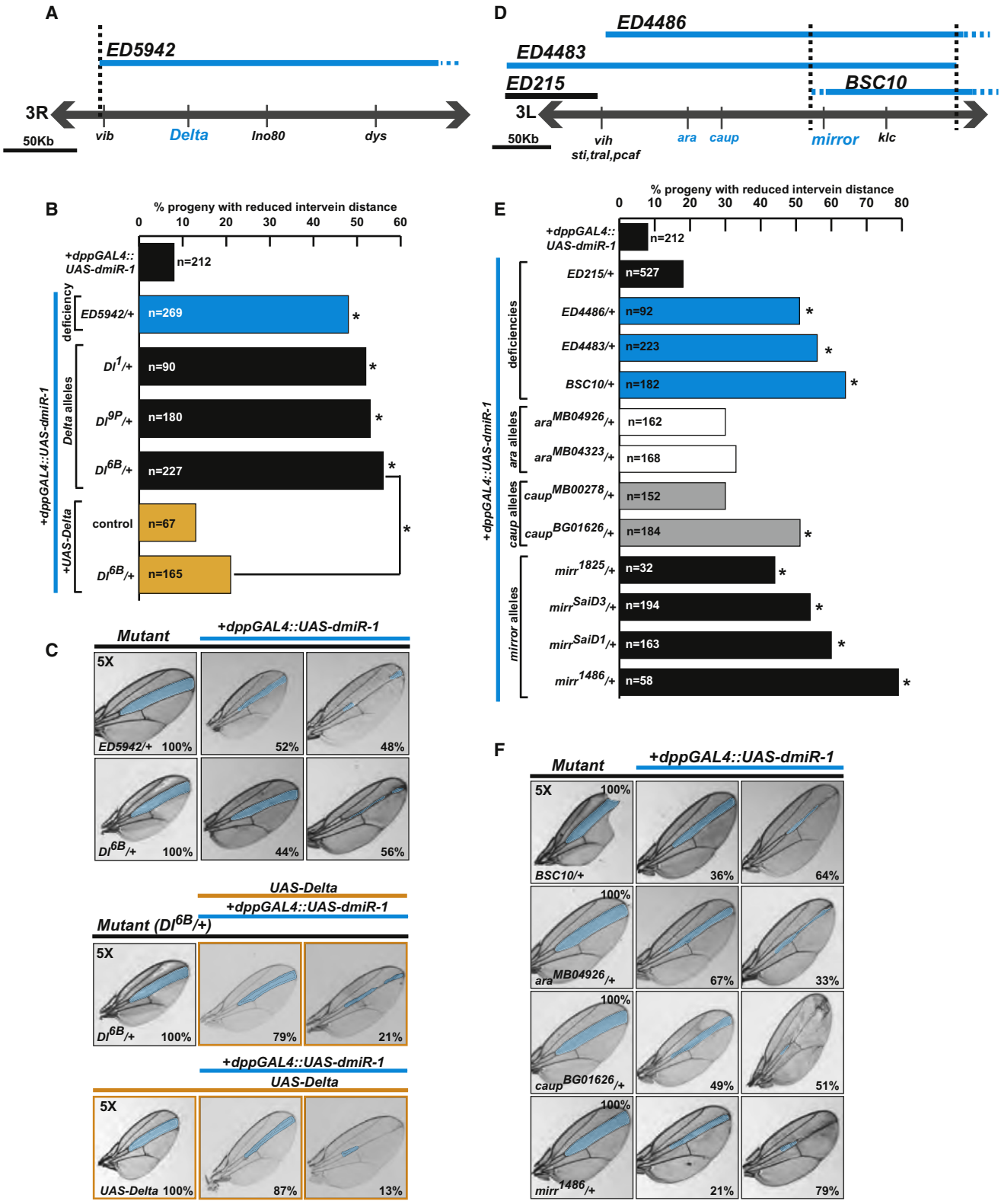

Figure 2. Validation of the *dmiR-1* Enhancer/Suppressor Genetic Screen

(A) Schematic of the deficiency ED5942 spanning *delta*.

(B) Percentages of affected offspring when specific deficiencies and alleles of *delta* were mated to the *dpp-GAL4::UAS-dmiR-1* line. Dl^{1}, Dl^{9P}, Dl^{6B} are loss of function alleles. Yellow bars depict rescue of enhancement as shown in the center panels of (C). *$p < 0.001$.

of *dmiR-1*, *kay*$^{[sro-1]}$, and wild-type *kay* resulted in rescue of the phenotype, and this was also true for the *kay*$^{[1]}$ and *kay*$^{[EY01644]}$ alleles (Figure 3C, E). We concluded that a decrease in *kay* function specifically enhanced the *dpp-GAL4::UAS-dmiR-1* wing phenotype.

To determine if *dmiR-1* reduced *kay* mRNA levels through direct targeting of the *kay* 3′ UTR, we introduced the full 3′ UTR into a luciferase reporter vector and transfected this with or without *dmiR-1* into fly S2 cells. We observed a dose-dependent reduction in luciferase activity in the presence of *dmiR-1*, signifying that *dmiR-1* likely directly regulates kay levels through the 3′ UTR (Figure 3F; Figure S3A). Mutation of two putative *dmiR-1* binding sites resulted in loss of *dmiR-1*-mediated repression, indicating functionality of these sites (Figure 3F; Figure S3B).

Genetic Interaction between *dmiR-1* and *kay* Depends on JNK-Mediated Signals

Kay modulates migration, cell polarity, and directionality cues within developing tissues (Riesgo-Escovar and Hafen, 1997; Zeitlinger et al., 1997, Weber et al., 2008), and *kay* null flies are nonviable. In contrast, mammals have multiple *kay* orthologs (*Fra1*, *Fra2*, *c-Fos*, *FosB*) that appear to be partially redundant (Fleischmann et al., 2000). As an immediate-early response gene, *c-Fos* is rapidly upregulated in the heart under a variety of pathological conditions (Izumo et al., 1988; Larsen et al., 1998) and modulates the genomic response to mechanical and cellular stress. Kay/c-Fos dimerizes with other proteins, such as c-Jun, to form the AP-1 complex. Kay/c-Fos is phosphorylated by both the Ras/MAPK and jun-kinase (JNK) pathways, resulting in distinct transcriptional responses.

We tested proteins within the Ras/MAPK, and JNK signaling pathways for a genetic interaction with *dmiR-1*. Mutants within the Ras/MAPK or JNK pathway did not genetically interact with *dmiR-1* to the same degree as *kay* in our wing-based assay (data not shown). Gain-of-function alleles predicted to activate Ras/MAPK, including one involving the epidermal-like growth factor receptor (EGFR), also did not consistently enhance the wing vein phenotype (data not shown).

To test these pathways in an alternative fashion, we utilized fly lines containing transgenes encoding mutants of *kay* that were resistant to phosphorylation by either JNK or MAPK kinases (gifts from D. Bohmann, University of Rochester). These UAS-based fly lines have putative JNK or RAS-MAPK phosphorylation sites in *kay* mutated to alanine residues, allowing segregation of JNK from RAS/MAPK signaling (Ciapponi et al., 2001). The mutant *UAS-kay*$^{[Pan-Ala]}$, which has all putative threonine (T) or serine (S) residues involved in phosphorylation mutated to alanine (A), resulted in high lethality when crossed to the *dpp-GAL4::UAS-dmiR-1* line (data not shown). The *UAS-kay*$^{[C-Ala]}$ mutant harboring alanine substitutions of RAS-MAPK-sensitive S/T residues in the carboxy-terminal region only mildly enhanced the *dpp-GAL4::UAS-dmiR-1* phenotype (Figures 3G and 3H bottom row). In contrast, *UAS-kay*$^{[N-Ala]}$, containing alanine substitutions of JNK-sensitive residues, recapitulated the loss of function alleles of *kay*, implying that phosphorylation of the JNK-sensitive residues was important for kay function in this assay (Figures 3G and 3H top row). These results provided evidence that JNK activity might be critical to the observed genetic interaction between *kay* and *dmiR-1*.

dmiR-1 Expression in the Wing Imaginal Disc Results in Trichome Misalignment

Dl, *mirr*, and *kay* have been implicated as members of the genetic network governing planar cell polarity (PCP) in *Drosophila* (Cooper and Bray, 1999; Fanto and Mlodzik, 1999; Weber et al., 2008). Cell polarity signals flow through the transmembrane receptor frizzled (fz), which associates with dishevelled (dsh) and strabismus/van gogh (Vang), to activate the JNK signaling cascade (Boutros et al., 1998; Weber et al., 2000). Core proteins within the PCP signaling cascade are highly conserved, and PCP in mammals is central to fundamental processes, such as gastrulation and organogenesis (for review, see Veeman et al., 2003, Wallingford et al., 2002, Zallen, 2007). In flies, PCP generates the stereotypical proximal-to-distal orientation of hairs and bristles over the ectoderm and, when disturbed, results in a whorled bristle pattern (Classen et al., 2005).

We hypothesized that *kay*, *Dl*, and *mirr* might have been identified in our screen in part due to a common functionality in the generation of cell polarity. To test this, we counted the number of misaligned hairs, or trichomes, in a standard location (boundaries marked in the anterior-posterior (A-P) dimension by L3 and L4 and in the proximal-distal (P-D) dimension by the posterior cross vein and anterior cross vein). Interestingly, in *dpp-GAL4::UAS-dmiR-1* flies, ~4% of wing hairs were not oriented in the normal P-D orientation, compared to 0.6% seen in wild-type animals (Figure 4). To determine if these results were specific to *dmiR-1*, the *dpp-GAL4* fly line was mated to a *UAS-miR-7* fly line (gift of E. Lai, Rockefeller University) to generate the control fly line *dpp-GAL4::UAS-dmiR-7*. The *dpp-GAL4::UAS-dmiR-7* fly line had numbers of misaligned trichomes closer to wild-type animals (0.18%), supporting the notion that *dmiR-1* specifically interferes with the generation of PCP (data not shown). We found that heterozygosity of *Dl*, *mirr*, or *kay* mutant alleles, along with *dmiR-1* expression, significantly increased the numbers of misaligned wing hairs when compared to wild-type or *dpp-*

(C) Panels of representative fly wings with the L3/L4 area highlighted in blue. Control parental mutant lines (*ED5942*, *Df*^{6B} *and UAS-delta)* shown to the left, with representative wings of pertinent offspring when crossed with the *dpp-GAL4::UAS-dmiR-1* line. Wings scored as "no change from *dpp-GAL4::UAS-dmiR-1*" (center) or "enhanced" (right), with percentages noted in bottom right corner. Yellow edged images: (top) *UAS-delta*, *Df*^{6B}, *dpp-GAL4::UAS-dmiR-1* representative fly wings displaying rescue of the phenotype, and the control *UAS-delta*, *dpp-GAL4::UAS-dmiR-1*, representative fly wings (bottom).
(D) Schematic of deficiencies containing the *Iroquois* locus: *araucan (ara)*, *caupolican (caup)*, *mirror (mirr)*. Blue lines: chromosomal location of deficiencies that enhance the *dpp-GAL4::UAS-dmiR-1* phenotype in ≥50% of progeny.
(E) Percentages of affected offspring when specific deficiencies (as in D), and loss of function alleles of the *Iroquois* locus (*ara*^{MB04926}, *ara*^{MB04323}, *caup*^{MB00278}, *caup*^{BG01626}, *mirr*^{1825}, *mirr*^{SaiD3}, *mirr*^{SaiD1}, *mirr*^{1486}) were mated to the *dpp-GAL4::UAS-dmiR-1* line. *p < 0.001.
(F) Control parental mutant lines (*BSC10*, *ara*^{MB04323}, *caup*^{BG01626}, *and mirr*^{1486}) shown to the left, with representative wings of pertinent offspring when crossed with the *dpp-GAL4::UAS-dmiR-1* line (as in E). Wings scored as "no change" (center) or "enhanced" (right), with percentages noted in bottom right corner.
See also Figures S1 and S2.

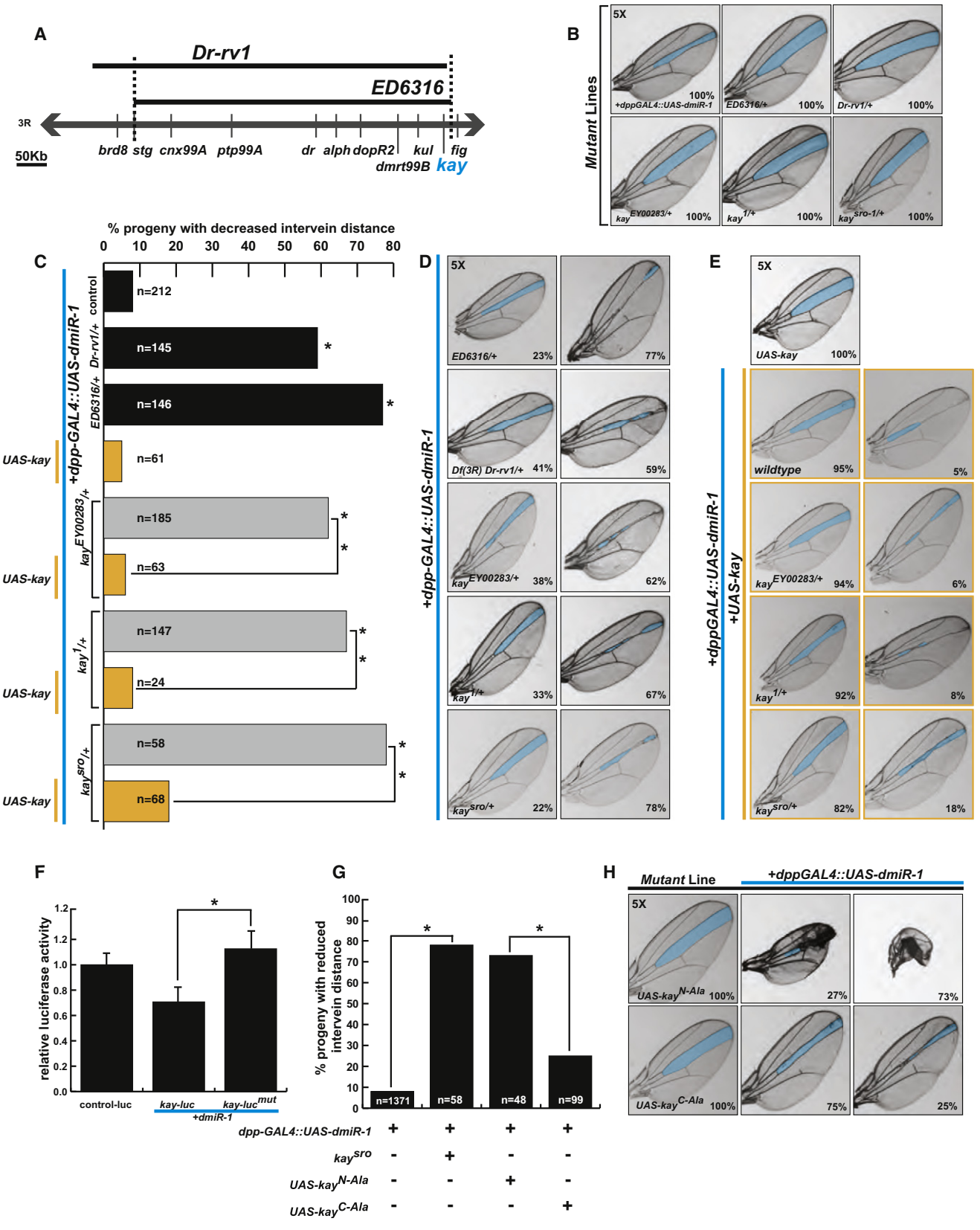
A
Dr-rv1
ED6316
3R
50Kb
brd8 stg cnx99A ptp99A dr alph dopR2 kul fig
dmrt99B kay
B
Mutant Lines
5X
+dppGAL4::UAS-dmiR-1
ED6316/+
Dr-rv1/+
kay EY00283/+
kay 1/+
kay sro-1/+
100%
C
% progeny with decreased intervein distance
0 10 20 30 40 50 60 70 80
+dpp-GAL4::UAS-dmiR-1
control
Dr-rv1/+
ED6316/+
kay EY00283/+
kay 1/+
kay sro/+
UAS-kay
n=212
n=145
n=146
n=61
n=185
n=63
n=147
n=24
n=58
n=68
D
+dpp-GAL4::UAS-dmiR-1
ED6316/+ 23% 77%
Df(3R) Dr-rv1/+ 41% 59%
kay EY00283/+ 38% 62%
kay 1/+ 33% 67%
kay sro/+ 22% 78%
E
+dppGAL4::UAS-dmiR-1
+UAS-kay
UAS-kay 100%
wildtype 95% 5%
kay EY00283/+ 94% 6%
kay 1/+ 92% 8%
kay sro/+ 82% 18%
F
relative luciferase activity
control-luc
kay-luc
kay-luc mut
+dmiR-1
G
% progeny with reduced intervein distance
n=1371
n=58
n=48
n=99
dpp-GAL4::UAS-dmiR-1
kay sro
UAS-kay N-Ala
UAS-kay C-Ala
H
Mutant Line
+dppGAL4::UAS-dmiR-1
UAS-kay N-Ala 100% 27% 73%
UAS-kay C-Ala 100% 75% 25%

GAL4::UAS-dmiR-1 flies (Figure 4; Figure S4A). In addition to being misaligned, many hairs were abnormally foreshortened and thickened (data not shown). Overexpression of *Dl* through the use of two *UAS-Dl* lines did not rescue the alignment defect (Figure S4B). In contrast, overexpression of *kay* (*UAS-kay*) rescued the wing PCP defects induced by expression of *dmiR-1* in the *kay* heterozygous background (Figure S4C).

dmiR-1 Genetically Interacts with Members of the Core PCP Pathway

To determine if trichome alignment defects might reflect *dmiR-1* regulation of core PCP proteins, we tested two members of this cascade that are bioinformatically predicted to be direct targets of *dmiR-1*: *van gogh (vang)* and *prickle (pk)* (Stark et al., 2003), as well as their upstream effector, *dishevelled (dsh).* When we tested alleles of *dsh*, *vang*, and *pk* in the intervein wing assay, we found that multiple alleles of these genes genetically interacted with *dmiR-1* (Figure S5A, right). Examination of the directionality of the wing hairs also demonstrated that multiple alleles of *dsh*, *vang*, and *pk* enhanced the effect of *dmiR-1* on PCP (Figure S5A, left). Interestingly, unlike our results for *Dl* and *kay*, the degree of effect on intervein distance for *pk* alleles did not predict the severity of PCP defects. These results indicate that the loss of intervein distance may be mechanistically distinct from the loss of PCP. Testing of the 3′ UTRs of both *vang* and *pk* in S2 cells indicated that *pk*, but not *vang*, is a direct target of *dmiR-1* (Figure S5B). We observed a dose-dependent reduction in *pk*-luciferase activity in the presence of *dmiR-1*, signifying that *dmiR-1* likely directly regulates *pk* levels through the 3′ UTR (Figure S5C). The latter results are consistent with *dmiR-1* regulating PCP on multiple levels (Figure S5D) and highlight the ability of our screen to identify genetic pathways regulated by *dmiR-1*.

Dysregulation of *dmiR-1* and *kay* in Fly Heart Results in Cell Polarity Defects

The artificial fly wing assay proved effective in discovering genetic interactions with *dmiR-1*, including those involving the *kay* and PCP pathways. *dmiR-1* is normally expressed in cardiac and somatic muscle, so we investigated whether the genetic relationships regarding PCP identified in the wing were present in areas of endogenous expression, in the absence of overexpression. The fly heart, or dorsal vessel, is segmentally patterned with a defined number of myocardial and pericardial cells, and expresses *dmiR-1* early in development (Kwon et al., 2005; Sokol and Ambros, 2005). In the dorsal vessel, Slit, a glycoprotein secreted from the medial surface of cardioblasts, acts as a polarity marker and signal by interacting with its receptor, roundabout (robo), to assure that cardioblasts migrate properly to the midline (Qian et al., 2005; Santiago-Martinez et al., 2006, MacMullin and Jacobs, 2006).

To determine if *dmiR-1* functions to regulate cell polarity within the fly heart, we analyzed *dmiR-1* null fly embryos *(Δ/ΔdmiR-1)* at stage 16. Immunostaining of these embryos for the cardioblast marker Neuromancer (Nmr) and for Slit revealed that 77% of embryos had misaligned cardioblasts and abnormally diffuse secretion of Slit from the medial and lateral sides of cardioblasts (Figures 5B and 5F). Parallel studies in embryos heterozygous for *dmiR-1* revealed 8% affected embryos, similar to wild-type embryos (Figure 5F). To determine if supraphysiologic levels of *dmiR-1* affected cardiac polarity, we used the *tinCΔ4-GAL4* driver (Lo and Frasch, 2001) to increase the levels of *dmiR-1* specifically within the fly heart. The resultant *tinCΔ4-GAL4::UAS-dmiR-1* embryos collected at 29° or 18°C also had diffuse Slit secretion, indicating that the dosage of *dmiR-1* within the fly heart was critical for normal cell polarity and cardioblast alignment (Figures 5C and 5G). Immunostaining for α-Spectrin, a second cardioblast polarity marker, in the same genotypes as described above was notable for disruption of the normal apical-lateral expression pattern, providing further evidence that cell polarity within the embryonic heart was disrupted (Figures S6B, S6C, S6F, and S6G).

We then determined if *kay* mutants also displayed cell specification or polarity abnormalities. We harvested homozygous $kay^{[1]}$ *and* $kay^{[Sro\text{-}1]}$ stage 16 embryos and immunostained for Nmr, Dmef2 (muscle progenitors), Tin (muscle progenitors), or Eve (pericardial cells) (Figure S7). We detected no significant differences in the numbers of cardioblasts or pericardial cells per hemisegment compared with wild-type. However, when we immunostained the homozygous $kay^{[1]}$ and $kay^{[Sro\text{-}1]}$ embryos for Nmr and Slit to evaluate the morphology of the heart tube, we found evidence of cardioblast misalignment and diffuse, but not reduced, expression of Slit from the medial and lateral sides of the cardioblasts (Figures 5D and 5H, data not shown). Immunostaining of homozygous $kay^{[1]}$ *and* $kay^{[Sro\text{-}1]}$ stage 16 embryos with α-Spectrin also revealed loss of the normal apical-lateral expression pattern of α-Spectrin (Figures S6D and S6H; data not

Figure 3. *Kayak* Genetically Interacts with *dmiR-1*

(A) Schematic of the deficiencies Df(3R) *Dr-rv-1* and Df(3R)*ED6316* spanning *kayak*.

(B) Panels of representative parental mutant fly wings with the L3/L4 area highlighted in blue. Note normal L3/L4 intervein distance.

(C) Percentages of affected offspring when specific deficiencies and mutant alleles of *kay* were mated to the *dpp-GAL4::UAS-dmiR-1* line. Yellow bars depict rescue of phenotypic enhancement with expression of *kay* (*UAS-kay*) as shown in (D and E). *$p < 0.001$.

(D) Representative wings of pertinent offspring when Df(3R) *Dr-rv-1* and Df(3R)*ED6316*, and the loss of function *kay* alleles ($kay^{EY00283}$, kay^{1}, kay^{sro}) were crossed with the *dpp-GAL4::UAS-dmiR-1* line. Wings scored as "no change" (left) or "enhanced" (right), with percentages noted in bottom right corner.

(E) Images of representative wings from a genetic rescue experiment. Top: control wing from a *UAS-kay* fly. Lower rows: Matings between *UAS-kay*, *dpp-GAL4::UAS-dmiR-1* flies and flies harboring heterozygous mutant alleles of *kay* ($kay^{EY01644}$, kay^{1}, kay^{sro}). Wings were scored as "no change" (left) or "enhanced" (right), with percentages noted in bottom right corner.

(F) Relative luciferase activity with or without the 3′ UTR of *kay* which was inserted into the 3′ UTR of a constitutively active luciferase vector in the presence or absence of *dmiR-1*. *Kay-luc*^{mut}: luciferase reporter with the two putative *dmiR-1* binding sites mutated as shown in Figure S3B. *$p < 0.05$. Error bars are represented as standard error of the mean.

(G) Percentage of affected offspring, comparing kay^{sro} mutants to mutants containing amino- and carboxy-terminal substitutions of serine and threonine residues to alanine. *$p < 0.001$.

(H) Photographs of representative wings for data in (G).

See also Figure S3.

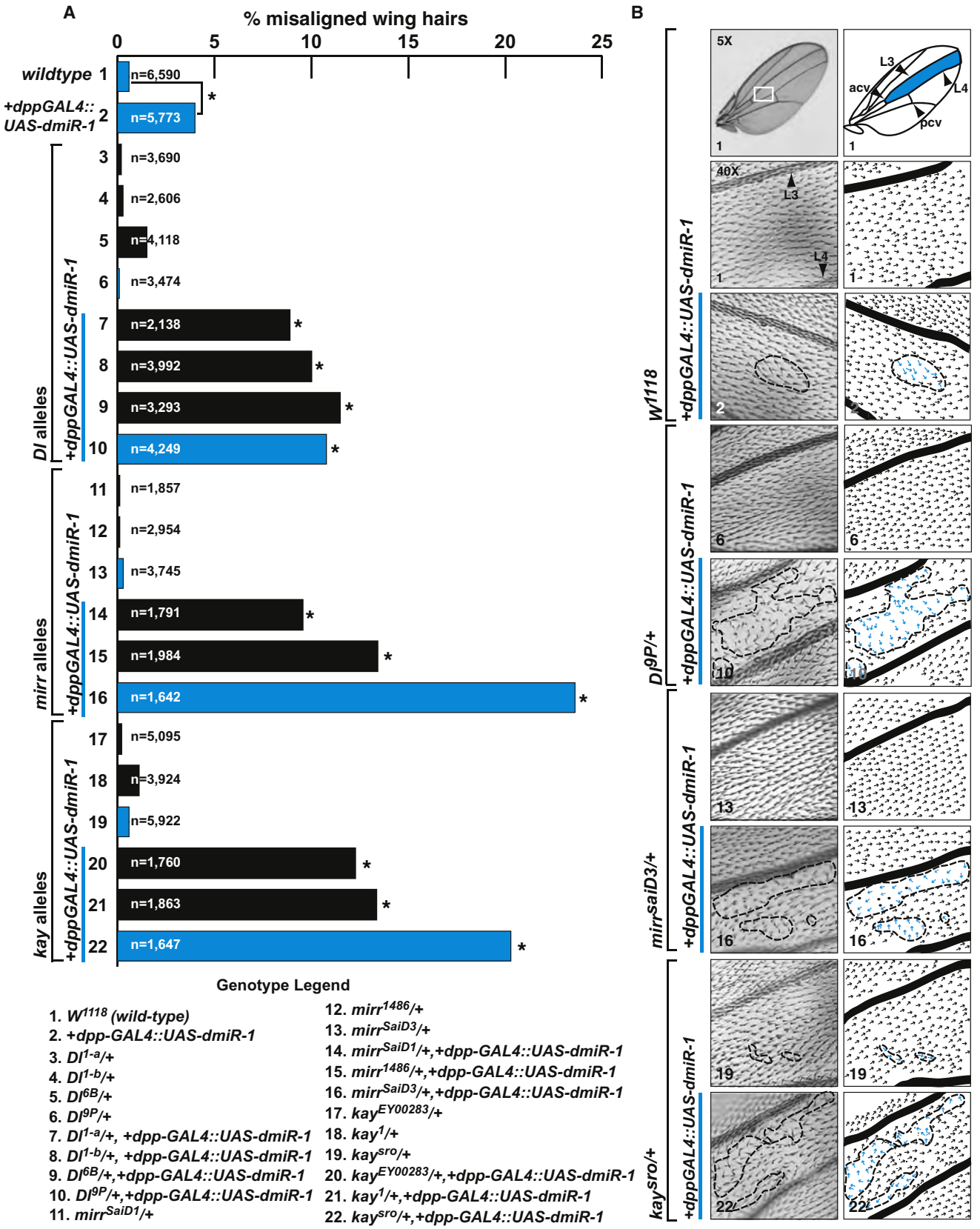
A
% misaligned wing hairs
0
5
10
15
20
25
wildtype 1
n=6,590
+dppGAL4::
UAS-dmiR-1 2
n=5,773
Dl alleles
+dppGAL4::UAS-dmiR-1
3 n=3,690
4 n=2,606
5 n=4,118
6 n=3,474
7 n=2,138
8 n=3,992
9 n=3,293
10 n=4,249
mirr alleles
+dppGAL4::UAS-dmiR-1
11 n=1,857
12 n=2,954
13 n=3,745
14 n=1,791
15 n=1,984
16 n=1,642
kay alleles
+dppGAL4::UAS-dmiR-1
17 n=5,095
18 n=3,924
19 n=5,922
20 n=1,760
21 n=1,863
22 n=1,647
Genotype Legend
1. W1118 (wild-type)
2. +dpp-GAL4::UAS-dmiR-1
3. Dl1-a/+
4. Dl1-b/+
5. Dl6B/+
6. Dl9P/+
7. Dl1-a/+, +dpp-GAL4::UAS-dmiR-1
8. Dl1-b/+, +dpp-GAL4::UAS-dmiR-1
9. Dl6B/+,+dpp-GAL4::UAS-dmiR-1
10. Dl9P/+,+dpp-GAL4::UAS-dmiR-1
11. mirrSaiD1/+
12. mirr1486/+
13. mirrSaiD3/+
14. mirrSaiD1/+,+dpp-GAL4::UAS-dmiR-1
15. mirr1486/+,+dpp-GAL4::UAS-dmiR-1
16. mirrSaiD3/+,+dpp-GAL4::UAS-dmiR-1
17. kayEY00283/+
18. kay1/+
19. kaysro/+
20. kayEY00283/+,+dpp-GAL4::UAS-dmiR-1
21. kay1/+,+dpp-GAL4::UAS-dmiR-1
22. kaysro/+,+dpp-GAL4::UAS-dmiR-1
B
W1118 +dppGAL4::UAS-dmiR-1
Dl9P/+ +dppGAL4::UAS-dmiR-1
mirrSaiD3/+ +dppGAL4::UAS-dmiR-1
kaysro/+ +dppGAL4::UAS-dmiR-1
5X
40X
L3
L4
acv
pcv

shown).These results indicated that kay function was necessary for normal dorsal vessel formation and cell polarity of cardioblasts but was not important for cell specification.

Since *kay* was a direct target of repression by *dmiR-1* and genetically interacted in the wing vein assay, we tested whether the heterozygosity of *kay* could mitigate the loss of *dmiR-1* in the developing heart. We found decreased *kay* activity from two different *kay* loss-of-function alleles reduced the penetrance of the *Δ/ΔdmiR-1* heart phenotype with respect to the diffuse medial and lateral expression of Slit (Figures 5E and 5I, data not shown). Furthermore, immunostaining of these doubly mutant embryos for α-Spectrin demonstrated that the normal apical-lateral expression pattern was partially restored in the *Δ/ΔdmiR-1* embryos heterozygous for *kay* (Figures S6E and S6I). These results suggested that a portion of the dosage effects of *dmiR-1* in the heart are due to abnormal kay activity.

Regulation of *c-Fos* and *c-Jun* Activity by *miR-1* in the Stressed Mammalian Heart

Our screen was based on the hypothesis that interrogation of the *Drosophila* genome for genetic partners of *dmiR-1* would yield insights into mammalian cardiac and skeletal muscle biology. To test our most promising candidates, we performed quantitative PCR (q-PCR) on cardiac mRNA obtained from 8-week-old mice overexpressing *miR-1* by threefold in the postnatal heart under control of the α-*MHC* promoter (α-*MHC-miR-1*) (Zhao et al., 2005, 2007). We found a statistically significant reduction in mRNA levels of *c-Fos*, *Delta-like-1*, *Irx4*, *−5*, and *-6* in *miR-1* transgenic mice (Figure 6A). These results provided evidence that our wing-based screen identified several genetic partners of *miR-1* that could be extrapolated to the mammalian heart, including some that are direct targets such as *Delta-like-1* and *Irx5* (Ivey et al., 2008; Zhao et al., 2007).

c-Fos is an immediate early response gene and is transiently upregulated in the first few hours after cardiac stress, such as that induced by pressure overload (Komuro et al., 1990; Schunkert et al., 1991). To determine how *c-Fos* and *miR-1* mRNA levels were regulated in the first few hours of increased afterload, we examined left ventricular gene expression from wild-type mice after thoracic aortic banding (TAB) at 1, 4, 8, 16, 24, and 48 hr postprocedure. *c-Fos* mRNA and *miR-1* levels increased dramatically, with peak *miR-1* levels coinciding with a precipitous decline in *c-Fos* mRNA levels in ventricular tissue (Figure 6B).

To determine if the increase of *miR-1* levels participated in the negative regulation of the immediate early gene response and might contribute to the rapid decrease in *c-Fos* expression, we performed TAB experiments on *miR-1-2* null mice. *miR-1-2* null animals have a 50% reduction in the amount of mature *miR-1* due to the presence of the redundant *miR-1-1* allele (Zhao et al., 2007). The temporal pattern for *c-Fos* expression was shifted from a normal peak at 8 hr, to a peak 4 hr postprocedure, and more significantly, *c-Fos* levels were ∼6-fold higher in *miR-1-2* mutants than in wild-type animals (Figure 6C, right panel). Conversely, transgenic mice overexpressing *miR-1* in cardiomyocytes had greater than 6-fold lower *c-Fos* mRNA levels after TAB, compared with wild-type (Figure 6C, right panel). A similar pattern was observed for *c-Jun* expression (Figure 6C, center panel). Interestingly, there were no significant differences in the levels or timing of expression for *c-Myc* (Figure 6C, left panel). Western blots performed on hearts harvested at the time points of maximal induction in *miR-1-2* null or *miR-1* transgenic animals confirmed our q-PCR results (Figure 6D,E). To determine if the dysregulation of *c-Fos* was specific to the myocyte population, we performed immunohistochemistry on heart sections from wild-type and transgenic *miR-1* overexpressing mice. The number of cardiomyocytes that expressed *c-Fos*, which was largely nuclear (Figure S8A), was significantly decreased in transgenic mice overexpressing *miR-1* in cardiomyocytes (α-*MHC-miR-1*). Unlike the direct targeting of *kayak* by *dmiR-1* in flies, the 3′ UTR of *c-Fos* was not responsive to *miR-1* (Figure S8B), suggesting conservation of the pathway regulated by *miR-1*, but divergence in the precise targets by which the miRNA exerts its biologic effects.

DISCUSSION

This study highlights the utility of using *Drosophila* to conduct genome-wide studies to identify genetic pathways in which miRNAs function. Using an in vivo biological assay, followed by genetic and biochemical studies, we uncovered several candidate genes subject to *dmiR-1* regulation. Importantly, we identified previously validated targets, which served as positive controls. Furthermore, we identified *miR-1*-responsive genes and pathways that functioned to regulate cell polarity during fly cardiogenesis and to appropriately limit the mammalian heart's response to stress.

We purposefully chose a very high threshold (enhancement of phenotype in ∼50% of progeny) as a cutoff for further evaluation, and therefore likely excluded many additional biologically relevant genetic partners of *dmiR-1*. As our studies relied on the wing-specific *dpp-GAL4* system, the interrogated genes only encompass those that are normally expressed in the intervein region between L3 and L4. Because many of the pathways that determine cell fate, position, and differentiation are used reiteratively in divergent tissues, the genome-wide screen with an artificial wing assay revealed genes relevant to cardiovascular biology. It would be of interest to use heart- and muscle-specific expression assays to perform analogous in vivo studies with muscle- or heart-based phenotypes as a primary endpoint. The results presented here highlight the results obtained from one genetic locus. Other loci of interest are the subject of ongoing studies.

Figure 4. Enhancement of *dmiR-1* PCP Defects by Haploinsufficiency of *delta*, *mirror*, and *kayak*

(A) Graphic of percentage of misaligned wing hairs with n = number of hairs counted, representing a minimum number of five individual animals. Genotypes detailed below. *p < 0.001. Blue bars denote genotypes represented by photographs in (B).

(B) Photographs of representative adult fly wings of noted genotypes with schematic of hair alignment (right). Top: W^{1118} (wild-type) wing with pertinent anatomical structures noted to right. White box: low magnification view of location where hair alignment was determined. Areas with misaligned wing hairs are outlined in a dashed line, with individual hairs of normal proximal-distal orientation (black) or misoriented (blue) indicated. Genotype noted in bottom left corner. See also Figures S4 and S5.

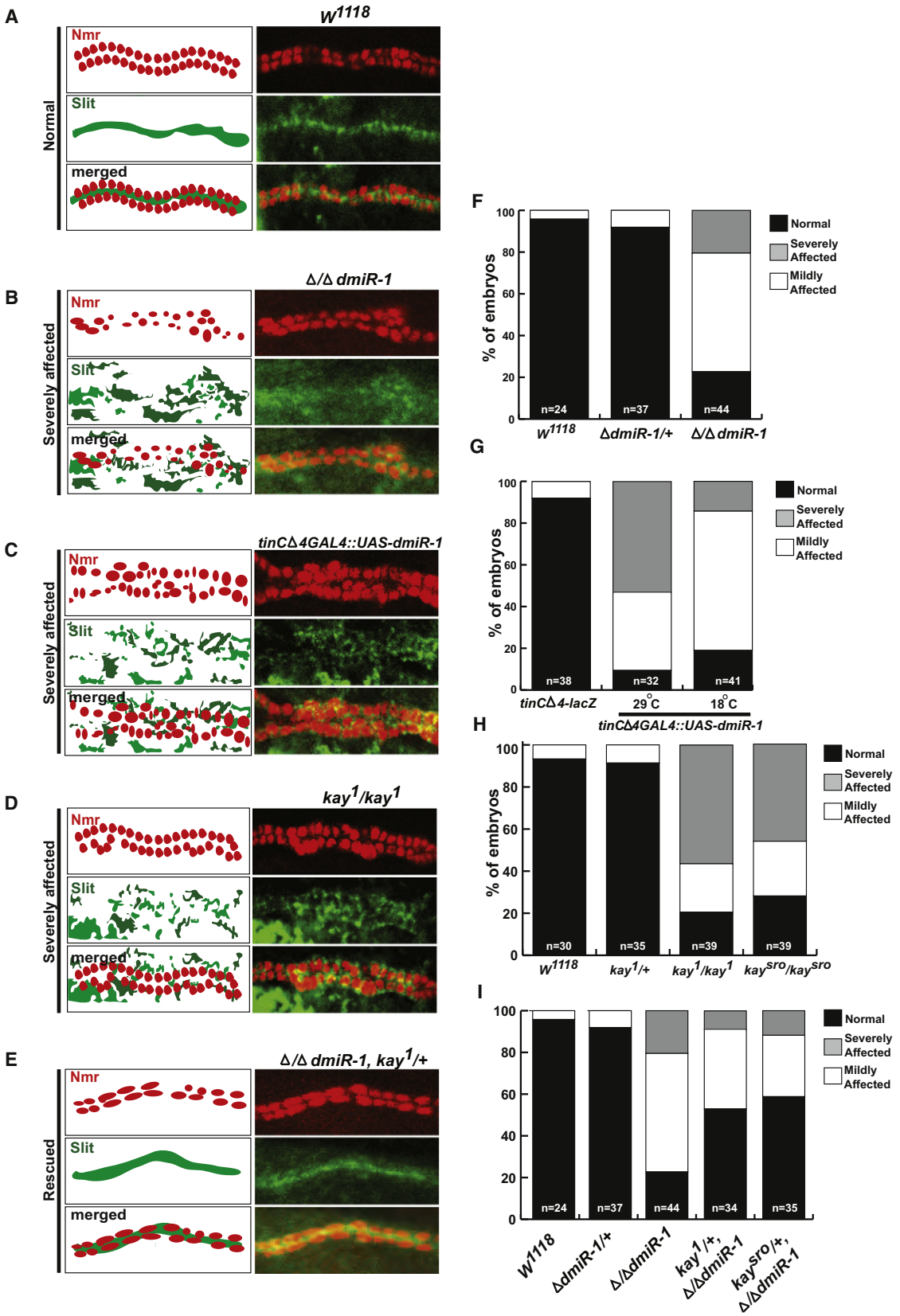
A
w^{1118}
Normal
Nmr
Slit
merged
B
Δ/Δ dmiR-1
Severely affected
C
tinCΔ4GAL4::UAS-dmiR-1
D
kay^1/kay^1
E
Δ/Δ dmiR-1, kay^1/+
Rescued
F
% of embryos
Normal
Severely Affected
Mildly Affected
n=24
n=37
n=44
w^{1118}
ΔdmiR-1/+
Δ/Δ dmiR-1
G
n=38
n=32
n=41
tinCΔ4-lacZ
29°C
18°C
tinCΔ4GAL4::UAS-dmiR-1
H
n=30
n=35
n=39
n=39
w^{1118}
kay^1/+
kay^1/kay^1
kay^{sro}/kay^{sro}
I
n=24
n=37
n=44
n=34
n=35
w^{1118}
ΔdmiR-1/+
Δ/ΔdmiR-1
kay^1/+, Δ/ΔdmiR-1
kay^{sro}/+, Δ/ΔdmiR-1

dmiR-1 Regulates Cardiac Cell Polarity in *Drosophila*

In addition to the loss of intervein distance, we found that *dmiR-1* overexpression also resulted in an increase in the frequency of misoriented wing hairs, consistent with defects in PCP. This led us to find that cell polarity within the *Drosophila* heart was also influenced by the dosage of *dmiR-1* and that aberrant *dmiR-1* activity resulted in defects in cardioblast alignment and the normal polarization of Slit and α-Spectrin expression in cardioblasts. These results suggest *dmiR-1* functions to generate or maintain cell polarity in the fly heart. It would be of interest to determine if *miR-1* modulation of PCP occurs primarily through modulation of *pk* and *JNK/kay/c-Fos*, or whether *miR-1*-mediated modulation of cytoskeletal proteins also plays a key role.

In mammals, cell polarization is emerging as an important process during the formation of the four-chambered heart and, in particular, the outflow tract of the heart. For example, mutations in the PCP genes *van gogh-like-2 (Vangl2/Looptail)* (Phillips et al., 2005, 2008), *scribbled (Scrib/Circletail)* (Phillips et al., 2007), and *dishevelled 2* (Hamblet et al., 2002) cause ventricular septal defects and outflow tract alignment defects. These defects have been partly attributed to aberrant migration of myocardial cells into the endocardial cushions. Interestingly, 50% of *miR-1-2* mutant embryos have ventricular septal defects that result in embryonic lethality (Zhao et al., 2007), and it will be interesting to determine if this is due to a PCP defect.

miR-1 and the Myocardial Response to Stress

From our pool of candidates, we chose to narrow our focus to the conserved genetic interaction between *miR-1* and the immediate-early gene, *c-Fos*. As *c-Fos* and *c-Jun* are induced by TAB, these transcription factors might mediate some of the adaptive transcriptional responses to stress. Unlike earlier studies that documented the downregulation of *miR-1* days after myocardial remodeling (Care et al., 2007, Sayed et al., 2007), we examined the relationship between *miR-1* and the immediate-early response genes induced within hours of banding the aorta. *miR-1*, *c-Fos*, and *c-Jun* were normally activated by TAB within a few hours, and in mice lacking *miR-1-2*, the initial upregulation of *c-Fos* and *c-Jun* was exaggerated in response to stress.

Our findings implicate *miR-1* in the initial dampening of stress response genes and in governing sets of genes used during periods of pressure overload. Serum response factor (SRF) is a direct upstream regulator of both *c-Fos* and *miR-1*, suggesting that *SRF* activates the transcriptional mediators of the immediate early gene response and, in a negative feedback loop, limits the extent of the stress response by activating *miR-1* expression. The 3′ UTR of *SRF* (Care et al., 2007) and *Elk-1* (K. Cordes and D. Srivastava, unpublished data), both necessary factors for *c-Fos* induction, are not subject to direct regulation by *miR-1*. Therefore, the mechanism by which *miR-1* modulates *c-Fos* levels in mammalian heart remains to be determined. However, previous studies have indicated that JNK signaling is activated during hypertrophic stimuli (Ramirez et. al 1997, Wang et al., 1998) and, in particular, is critical to the activity of TCF/Elk-1 on the *c-Fos* promoter (Cavigelli et al., 1995). Therefore, it is possible that in the murine heart, *miR-1* modulation of JNK activity may indirectly affect *c-Fos* levels through changes in the phosphorylation of TCF/Elk-1 (Figure S8C). It is intriguing that, over millions of years of evolution, the networks regulated by a miRNA can be conserved, but by virtue of the myriad targets of a miRNA, the points at which a miRNA can impinge on the network may diverge. Analogous to what we observe here, *miR-1* directly targets the cardiac developmental transcription factor, Hand2, in mice but not in flies, yet regulates cardiogenesis in both species (Zhao et al., 2005; Kwon et al., 2005; Han et al., 2006). It will be interesting to determine if this is a common feature in the evolutionary development of miRNA-mediated gene regulation.

EXPERIMENTAL PROCEDURES

Drosophila Stocks

Flies with genomic deletions (deficiencies) were ordered from Bloomington Stock Center (Bloomington, IN) and DrosDel (Cambridge, UK). The following fly lines were generously provided by their creators: ΔdmiR-1 (C. Kwon, Gladstone Institute, San Francisco), UAS-dmiR-7 (Eric Lai, Sloan-Kettering Institute, New York). Fly lines not specifically mentioned in the text were obtained from the Bloomington Stock Center. Wild-type control flies are W^{1118}. Overexpression of transgenes was achieved using the UAS-GAL4 system (Brand and Perrimon, 1993). The following Gal4 and UAS lines were used: *dpp*-GAL4 (Bloomington Stock Center), *tinCΔ4*-GAL4 (R. Bodmer, Burnham Institute, La Jolla, CA), *UAS-kay*$^{[N\text{-}Ala]}$, *UAS-kay*$^{[C\text{-}Ala]}$ (D. Bohmann, University of Rochester, Rochester, New York).

Wing Hair Polarity Scoring

Flies were anesthetized with CO_2 and euthanized with isopropanol. Wings were removed and mounted on histology slides with Canada Balsam (Sigma). Hairs were counted at 20× magnification with ImagePro software (MediaCybernetics), and misaligned hairs were scored manually. A minimum of five animals per genotype were assayed.

Immunohistochemistry

Antibody staining was performed as described (Han et al., 2002). Cy3- or FITC-conjugated secondary antibodies (Jackson Laboratory) were used for fluorescent confocal microscopy. All the secondary antibodies were used at 1:200. Embryos with fluorescent staining were mounted in VectaShield (Vector Laboratories)

Figure 5. *dmiR-1* Influences Cell Polarity in the *Drosophila* Heart

(A) Schematic of the expression pattern for Neuromancer (Nmr, red) and Slit (green) in wild-type (W^{1118}) *Drosophila* hearts (left). Confocal images showing Nmr and Slit localization by immunostaining within the fly heart in wild-type (W^{1118}) stage 16 embryos (right).
(B) Schematic (left) and confocal (right) images of homozygous null *dmiR-1* stage 16 embryos, with Nmr and Slit expression in red and green, respectively.
(C) Schematic (left) and confocal (right) images of *tinCΔ4GAL4::UASdmiR-1* stage 16 embryos, with Nmr and Slit expression in red and green, respectively.
(D) Schematic (left) and confocal (right) images of homozygous mutant kay^1 stage 16 embryos, with Nmr and Slit expression in red and green, respectively.
(E) Schematic (left) and confocal (right) images of homozygous null *dmiR-1*, kay^1/+ stage 16 embryos, with Nmr and Slit expression in red and green, respectively.
(F) Quantification of (B) with normal (black), mildly (white), or severely (gray) affected embryos, according to genotype. Scoring was based on the degree of misalignment of the cardioblasts and diffuse expression of Slit.
(G) Quantification of (C) with normal (black), mildly (white), or severely (gray) affected embryos, according to genotype and temperature.
(H) Quantification of (D) with normal (black), mildly (white), or severely (gray) affected embryos, according to genotype.
(I) Quantification of (E) with normal (black), mildly (white), or severely (gray) affected embryos, according to genotype.
See also Figures S6 and S7.

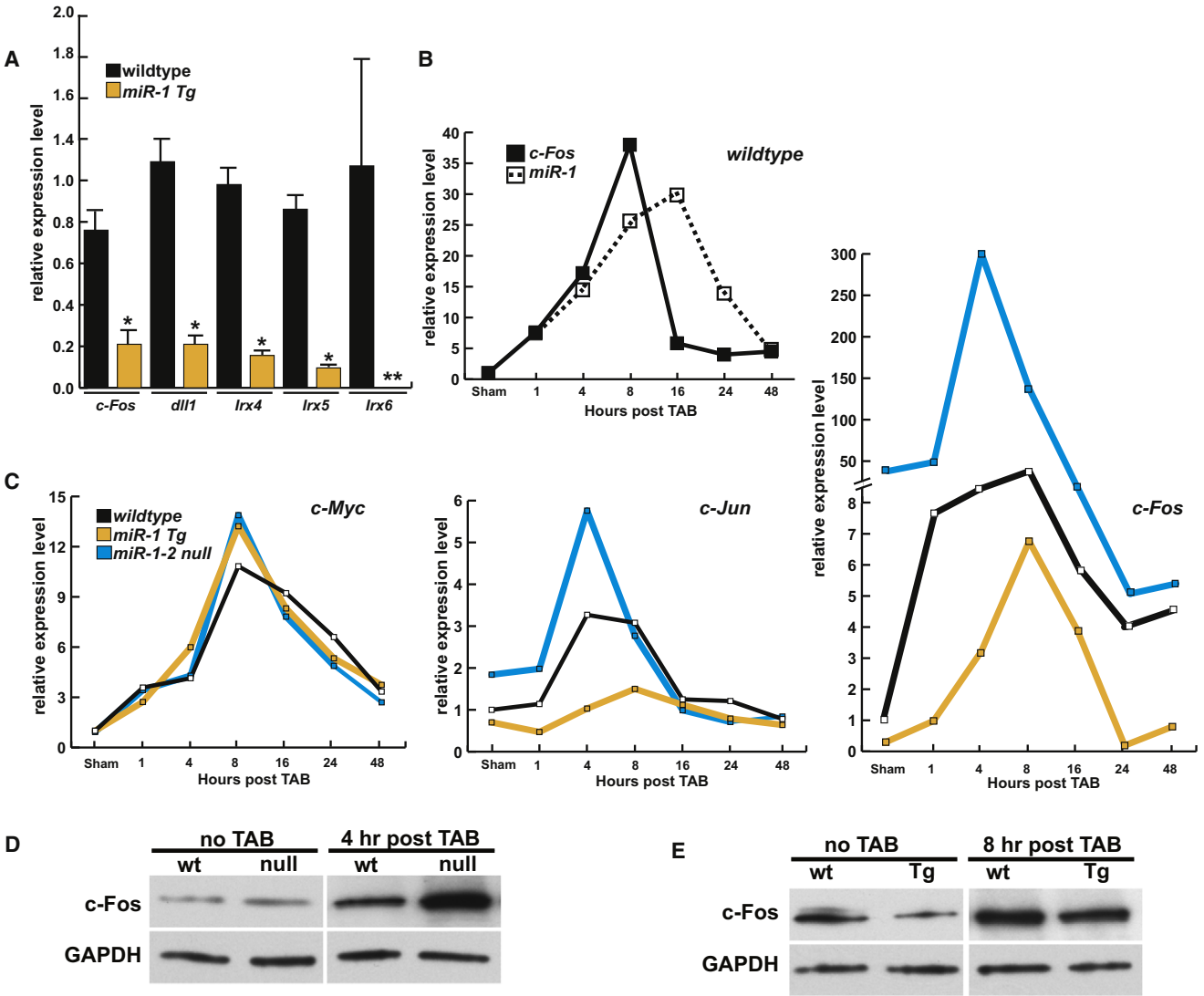

Figure 6. *miR-1-2* Limits Stress-Induced Activation of the *kay* Ortholog, *c-Fos*, in Mouse Hearts

(A) Quantification of mRNA levels for mouse orthologs of genes found to have a genetic interaction with *dmiR-1* in wild-type (black) or α-MHC-*miR-1* transgenic (Tg) mice (yellow). *p = < 0.05. *dll1:delta-like-1*, *lrx4,5,6: Iroquois* family 4,5,6. All values normalized to GAPDH levels. **Not detectable. n = 4 animals for each time point. Error bars are represented as standard error of the mean.

(B) Time course of *c-Fos* or *miR-1* expression after thoracic aortic banding (TAB) by qPCR in wild-type mice.

(C) Time course of *c-myc* (left), *c-Jun* (middle) and *c-Fos* (right) expression as determined by qPCR analysis after TAB. Wild-type animals (black), α-*MHC-miR-1* transgenic mice (yellow) and *miR-1-2* null (blue) mice are indicated.

(D–E) Western blots of mouse hearts at time points of maximal *c-Fos* induction in *miR-1-2* null (ko) (D) or α-*MHC-miR-1* transgenic (Tg) animals (E) after TAB.

and preparations were analyzed using Zeiss LSM510 and Biorad MRC-1024MP confocal microscopes. The following primary antibodies were used in this study: rabbit anti-Tinman, 1:1000 (Venkatesh et al., 2000); rabbit anti-β-galactosidase, 1:2000 (Invitrogen); mouse anti-β-galactosidase, 1:500 (Sigma); rabbit anti-DMef2, 1:2000 (Lilly et al., 1995); rabbit anti-Nmr, 1:500 (Leal et al., 2009); mouse anti-Slit 1:500 (Hybridoma Bank, Univ. of Iowa); rabbit anti-Eve, 1:300 (Frasch et al., 1987). c-Fos 1:200 (Santa Cruz) and α-Actinin antibody 1:800 (Sigma) were used for immunohistochemistry of mouse heart sections.

Thoracic Aortic Banding Model

The protocol was approved by institutional guidelines (University of California, San Francisco). Mice (8 weeks old) were anesthetized with 2.4% isoflurane/97.6% oxygen and placed in a supine position on a heating pad (37°C). Animals were intubated with a 19G stump needle and ventilated with room air with a MiniVent Type 845 mouse ventilator (Hugo Sachs Elektronik-Harvard Apparatus, Germany; stroke volume 250 μl, respiratory rate 120 breaths per minute). Pressure overload was induced by TAB. A 3-mm left-sided thoracotomy was created at the second intercostal space. The transverse aortic arch was ligated (7-0 Prolene) between the innominate and left common carotid arteries with an overlying 27 gauge needle. The needle was removed, leaving a discrete region of stenosis. The chest was closed, and the left-sided pneumothorax was evacuated. Some mice were subjected to a sham operation in which the aortic arch was visualized but not banded. Perioperative (24 hr) mortality was <10%.

Quantitative Real-Time PCR

For mouse q-PCR, RNA was extracted by TRizol method (Invitrogen) from individual hearts. q-PCR was performed using the Superscript III first-strand

synthesis system (Invitrogen). q-PCR was performed using the ABI 7900HT (TaqMan, Applied Biosystems), per the manufacturer's protocols. Optimized primers from Taqman Gene Expression Array were used. miRNA RT was conducted using the Taqman MicroRNA Reverse Transcription Kit (Applied Biosystems). miRNA q-RT-PCR was performed per the manufacturer's protocols by using primers from Taqman MicroRNA Assays (Applied Biosystems). Expression levels were normalized to GAPDH expression and U6 (microRNA q-PCR).

Western Blots

Western blots were performed as described (Zhao et al., 2005). Rabbit anti-c-c-Fos (Cell Signaling) and rabbit anti-GAPDH (Santa Cruz) were used at 1:1000 dilutions for western blots. All western blots were quantified using Alpha imager software from Alpha Innovations.

Statistics

Analysis of the rates of enhancement or suppression in the genomic screen were analyzed using the chi-square test. Luciferase assays, q-PCR, and quantification of immunohistochemistry were analyzed using the one-way Student's t test. Error bars are represented as standard error of the mean. Sample numbers were indicated in corresponding figures.

S2 Luciferase Assays

S2 cells were maintained at room temperature in Schneider's *Drosophila* Medium (GIBCO) supplemented with 10% FBS. Effectene Transfection Reagent (QIAGEN) was used for each transfection according to QIAGEN's protocol. For each well of a 24-well plate, 200 ng of pGL3-target (e.g., *kay*) 3′ UTR, pUAS-*dmiR-1*, pMT-*GAL4* and 50 ng of Renilla were transfected, along with vector only as a negative control. Luciferase assays were performed as described with the Dual-Luciferase Reporter Assay System (Promega).

SUPPLEMENTAL INFORMATION

Supplemental Information includes eight figures and one table and can be found with this article online at doi:10.1016/j.devcel.2011.03.010.

ACKNOWLEDGMENTS

We thank E. Lai, G. Rubin, and D. Bohmann for the fly lines as noted in the text, and F. Gao for providing selected fly stocks from the DrosDel collection and advice. We thank I. S. Kathiriya for critically reviewing the manuscript, and K. Cordes for sharing unpublished results. We thank all the members from the Srivastava lab for helpful discussion. I.N.K. is supported by 5K08HL079260-4. L.Q. is a Scholar of the California Institute for Regenerative Medicine (CIRM) and is a Lynda and Stewart Resnick Fellow. D.S. was supported by grants from NHLBI/NIH, the CIRM, and the Younger Family Foundation. This work was supported by NIH/NCRR grant (C06 RR018928) to the Gladstone Institute.

Received: June 29, 2010
Revised: January 21, 2011
Accepted: March 13, 2011
Published: April 18, 2011

REFERENCES

Bao, Z.Z., Bruneau, B.G., Seidman, J.G., Seidman, C.E., and Cepko, C.L. (1999). Regulation of chamber-specific gene expression in the developing heart by Irx4. Science *283*, 1161–1164.

Bartel, D.P. (2009). MicroRNAs: target recognition and regulatory functions. Cell *136*, 215–233.

Bernstein, E., Kim, S.Y., Carmell, M.A., Murchison, E.P., Alcorn, H., Li, M.Z., Mills, A.A., Elledge, S.J., Anderson, K.V., and Hannon, G.J. (2003). Dicer is essential for mouse development. Nat. Genet. *35*, 215–217.

Boutros, M., Paricio, N., Strutt, D.I., and Mlodzik, M. (1998). Dishevelled activates JNK and discriminates between JNK pathways in planar polarity and wingless signaling. Cell *94*, 109–118.

Brand, A.H., and Perrimon, N. (1993). Targeted gene expression as a means of altering cell fates and generating dominant phenotypes. Development *118*, 401–415.

Bray, S.J. (2006). Notch signalling: a simple pathway becomes complex. Nat. Rev. Mol. Cell Biol. *7*, 678–689.

Care, A., Catalucci, D., Felicetti, F., Bonci, D., Addario, A., Gallo, P., Bang, M.L., Segnalini, P., Gu, Y., Dalton, N.D., et al. (2007). MicroRNA-133 controls cardiac hypertrophy. Nat. Med. *13*, 613–618.

Cavigelli, M., Dolfi, F., Claret, F.X., and Karin, M. (1995). Induction of c-fos expression through JNK-mediated TCF/Elk-1 phosphorylation. EMBO J. *14*, 5957–5964.

Cavodeassi, F., Modolell, J., and Gomez-Skarmeta, J.L. (2001). The Iroquois family of genes: from body building to neural patterning. Development *128*, 2847–2855.

Chen, J.F., Mandel, E.M., Thomson, J.M., Wu, Q., Callis, T.E., Hammond, S.M., Conlon, F.L., and Wang, D.Z. (2006). The role of microRNA-1 and microRNA-133 in skeletal muscle proliferation and differentiation. Nat. Genet. *38*, 228–233.

Ciapponi, L., Jackson, D.B., Mlodzik, M., and Bohmann, D. (2001). Drosophila Fos mediates ERK and JNK signals via distinct phosphorylation sites. Genes Dev. *15*, 1540–1553.

Classen, A.-K., Anderson, K.I., Marois, E., and Eaton, S. (2005). Hexagonal packing of Drosophila wing epithelial cells by the planar cell polarity pathway. Dev. Cell *9*, 805–817.

Cooper, M.T., and Bray, S.J. (1999). Frizzled regulation of Notch signalling polarizes cell fate in the Drosophila eye. Nature *397*, 526–530.

Cordes, K.R., and Srivastava, D. (2009). MicroRNA regulation of cardiovascular development. Circ. Res. *104*, 724–732.

Costantini, D.L., Arruda, E.P., Agarwal, P., Kim, K.H., Zhu, Y., Zhu, W., Lebel, M., Cheng, C.W., Park, C.Y., Pierce, S.A., et al. (2005). The homeodomain transcription factor Irx5 establishes the mouse cardiac ventricular repolarization gradient. Cell *123*, 347–358.

Croce, C.M. (2009). Causes and consequences of microRNA dysregulation in cancer. Nat. Rev. Genet. *10*, 704–714.

Fanto, M., and Mlodzik, M. (1999). Asymmetric Notch activation specifies photoreceptors R3 and R4 and planar polarity in the Drosophila eye. Nature *397*, 523–526.

Fleischmann, A., Hafezi, F., Elliott, C., Remé, C.E., Rüther, U., and Wagner, E.F. (2000). Fra-1 replaces c-Fos-dependent functions in mice. Genes Dev. *14*, 2695–2700.

Frasch, M., Hoey, T., Rushlow, C., Doyle, H., and Levine, M. (1987). Characterization and localization of the even-skipped protein of Drosophila. EMBO J. *6*, 749–759.

Garcia-Bellido, A., Cortes, F., and Milan, M. (1994). Cell interactions in the control of size in Drosophila wings. Proc. Natl. Acad. Sci. USA *91*, 10222–10226.

Hamblet, N.S., Lijam, N., Ruiz-Lozano, P., Wang, J., Yang, Y., Luo, Z., Mei, L., Chien, K.R., Sussman, D.J., and Wynshaw-Boris, A. (2002). Dishevelled 2 is essential for cardiac outflow tract development, somite segmentation and neural tube closure. Development *129*, 5827–5838.

Han, Z., Fujioka, M., Su, M., Liu, M., Jaynes, J.B., and Bodmer, R. (2002). Transcriptional integration of competence modulated by mutual repression generates cell-type specificity within the cardiogenic mesoderm. Dev. Biol. *252*, 225–240.

Han, Z., Yi, P., Li, X., and Olson, E.N. (2006). Hand, an evolutionarily conserved bHLH transcription factor required for Drosophila cardiogenesis and hematopoiesis. Development *133*, 1175–1182.

Ikeda, S., He, A., Kong, S.W., Lu, J., Bejar, R., Bodyak, N., Lee, K.-H., Ma, Q., Kang, P.M., Golub, T.R., et al. (2009). MicroRNA-1 negatively regulates expression of the hypertrophy-associated Calmodulin and Mef2a genes. Mol. Cell. Biol. *29*, 2193–2204.

Inui, M., Martello, G., and Piccolo, S. (2010). MicroRNA control of signal transduction. Nat. Rev. Mol. Cell Biol. *11*, 252–263.

Ivey, K.N., Muth, A., Arnold, J., King, F.W., Yeh, R.F., Fish, J.E., Hsiao, E.C., Schwartz, R.J., Conklin, B.R., Bernstein, H.S., et al. (2008). MicroRNA regulation of cell lineages in mouse and human embryonic stem cells. Cell Stem Cell *2*, 219–229.

Izumo, S., Nadal-Ginard, B., and Mahdavi, V. (1988). Protooncogene induction and reprogramming of cardiac gene expression produced by pressure overload. Proc. Natl. Acad. Sci. USA *85*, 339–343.

Komuro, I., Kaida, T., Shibazaki, Y., Kurabayashi, M., Katoh, Y., Hoh, E., Takaku, F., and Yazaki, Y. (1990). Stretching cardiac myocytes stimulates protooncogene expression. J. Biol. Chem. *265*, 3595–3598.

Kwon, C., Han, Z., Olson, E.N., and Srivastava, D. (2005). MicroRNA1 influences cardiac differentiation in Drosophila and regulates Notch signaling. Proc. Natl. Acad. Sci. USA *102*, 18986–18991.

Larsen, T.H., Skar, R., Frotjold, E.K., Haukanes, K., Greve, G., and Saetersdal, T. (1998). Regional activation of the immediate-early response gene c-Fos in infarcted rat hearts. Int. J. Exp. Pathol. *79*, 163–172.

Leal, S.M., Qian, L., Lacin, H., Bodmer, R., and Skeath, J.B. (2009). Neuromancer1 and Neuromancer2 regulate cell fate specification in the developing embryonic CNS of Drosophila melanogaster. Dev. Biol. *325*, 138–150.

Lilly, B., Zhao, B., Ranganayakulu, G., Paterson, B.M., Schulz, R.A., and Olson, E.N. (1995). Requirement of MADS domain transcription factor D-MEF2 for muscle formation in Drosophila. Science *267*, 688–693.

Lo, P.C., and Frasch, M. (2001). A role for the COUP-TF-related gene seven-up in the diversification of cardioblast identities in the dorsal vessel of Drosophila. Mech. Dev. *104*, 49–60.

MacMullin, A., and Jacobs, J.R. (2006). Slit coordinates cardiac morphogenesis in Drosophila. Dev. Biol. *293*, 154–164.

Mendell, J.T. (2005). MicroRNAs: critical regulators of development, cellular physiology and malignancy. Cell Cycle *4*, 1179–1184.

Phillips, H.M., Murdoch, J.N., Chaudhry, B., Copp, A.J., and Henderson, D.J. (2005). Vangl2 acts via RhoA signaling to regulate polarized cell movements during development of the proximal outflow tract. Circ. Res. *96*, 292–299.

Phillips, H.M., Rhee, H.J., Murdoch, J.N., Hildreth, V., Peat, J.D., Anderson, R.H., Copp, A.J., Chaudhry, B., and Henderson, D.J. (2007). Disruption of planar cell polarity signaling results in congenital heart defects and cardiomyopathy attributable to early cardiomyocyte disorganization. Circ. Res. *101*, 137–145.

Phillips, H.M., Hildreth, V., Peat, J.D., Murdoch, J.N., Kobayashi, K., Chaudhry, B., and Henderson, D.J. (2008). Non-cell-autonomous roles for the planar cell polarity gene Vangl2 in development of the coronary circulation. Circ. Res. *102*, 615–623.

Qian, L., Liu, J., and Bodmer, R. (2005). Slit and Robo control cardiac cell polarity and morphogenesis. Curr. Biol. *15*, 2271–2278.

Ramirez, M.T., Sah, V.P., Zhao, X.L., Hunter, J.J., Chien, K.R., and Brown, J.H. (1997). The MEKK-JNK pathway is stimulated by alpha1-adrenergic receptor and ras activation and is associated with in vitro and in vivo cardiac hypertrophy. J. Biol. Chem. *272*, 14057–14061.

Riesgo-Escovar, J.R., and Hafen, E. (1997). Drosophila Jun kinase regulates expression of decapentaplegic via the ETS-domain protein Aop and the AP-1 transcription factor DJun during dorsal closure. Genes Dev. *11*, 1717–1727.

Ryder, E., Ashburner, M., Bautista-Llacer, R., Drummond, J., Webster, J., Johnson, G., Morley, T., Chan, Y.S., Blows, F., Coulson, D., et al. (2007). The DrosDel deletion collection: a Drosophila genomewide chromosomal deficiency resource. Genetics *177*, 615–629.

Santiago-Martinez, E., Soplop, N.H., and Kramer, S.G. (2006). Lateral positioning at the dorsal midline: Slit and Roundabout receptors guide Drosophila heart cell migration. Proc. Natl. Acad. Sci. USA *103*, 12441–12446.

Sayed, D., Hong, C., Chen, I.Y., Lypowy, J., and Abdellatif, M. (2007). MicroRNAs play an essential role in the development of cardiac hypertrophy. Circ. Res. *100*, 416–424.

Schunkert, H., Jahn, L., Izumo, S., Apstein, C.S., and Lorell, B.H. (1991). Localization and regulation of c-Fos and c-Jun protooncogene induction by systolic wall stress in normal and hypertrophied rat hearts. Proc. Natl. Acad. Sci. USA *88*, 11480–11484.

Sokol, N.S., and Ambros, V. (2005). Mesodermally expressed Drosophila microRNA-1 is regulated by Twist and is required in muscles during larval growth. Genes Dev. *19*, 2343–2354.

Stark, A., Brennecke, J., Russell, R.B., and Cohen, S.M. (2003). Identification of Drosophila MicroRNA targets. PLoS Biol. *1*, E60.

Veeman, M.T., Axelrod, J.D., and Moon, R.T. (2003). A second canon. Functions and mechanisms of beta-catenin-independent Wnt signaling. Dev. Cell *5*, 367–377.

Venkatesh, T.V., Park, M., Ocorr, K., Nemaceck, J., Golden, K., Wemple, M., and Bodmer, R. (2000). Cardiac enhancer activity of the homeobox gene tinman depends on CREB consensus binding sites in Drosophila. Genesis *26*, 55–66.

Wallingford, J.B., Fraser, S.E., and Harland, R.M. (2002). Convergent extension: the molecular control of polarized cell movement during embryonic development. Dev. Cell *2*, 695–706.

Wang, Y., Su, B., Sah, V.P., Brown, J.H., Han, J., and Chien, K.R. (1998). Cardiac hypertrophy induced by mitogen-activated protein kinase kinase 7, a specific activator for c-Jun NH2-terminal kinase in ventricular muscle cells. J. Biol. Chem. *273*, 5423–5426.

Weber, U., Paricio, N., and Mlodzik, M. (2000). Jun mediates Frizzled-induced R3/R4 cell fate distinction and planar polarity determination in the Drosophila eye. Development *127*, 3619–3629.

Weber, U., Pataki, C., Mihaly, J., and Mlodzik, M. (2008). Combinatorial signaling by the Frizzled/PCP and Egfr pathways during planar cell polarity establishment in the Drosophila eye. Dev. Biol. *316*, 110–123.

Williams, A.H., Liu, N., van Rooij, E., and Olson, E.N. (2009). MicroRNA control of muscle development and disease. Curr. Opin. Cell Biol. *21*, 461–469.

Xu, C., Lu, Y., Pan, Z., Chu, W., Luo, X., Lin, H., Xiao, J., Shan, H., Wang, Z., and Yang, B. (2007). The muscle-specific microRNAs miR-1 and miR-133 produce opposing effects on apoptosis by targeting HSP60, HSP70 and caspase-9 in cardiomyocytes. J. Cell Sci. *120*, 3045–3052.

Yang, B., Lin, H., Xiao, J., Lu, Y., Luo, X., Li, B., Zhang, Y., Xu, C., Bai, Y., Wang, H., et al. (2007). The muscle-specific microRNA miR-1 regulates cardiac arrhythmogenic potential by targeting GJA1 and KCNJ2. Nat. Med. *13*, 486–491.

Zallen, J.A. (2007). Planar polarity and tissue morphogenesis. Cell *129*, 1051–1063.

Zeitlinger, J., Kockel, L., Peverali, F.A., Jackson, D.B., Mlodzik, M., and Bohmann, D. (1997). Defective dorsal closure and loss of epidermal decapentaplegic expression in Drosophila fos mutants. EMBO J. *16*, 7393–7401.

Zhao, Y., Samal, E., and Srivastava, D. (2005). Serum response factor regulates a muscle-specific microRNA that targets Hand2 during cardiogenesis. Nature *436*, 214–220.

Zhao, Y., Ransom, J.F., Li, A., Vedantham, V., von Drehle, M., Muth, A.N., Tsuchihashi, T., McManus, M.T., Schwartz, R.J., and Srivastava, D. (2007). Dysregulation of cardiogenesis, cardiac conduction, and cell cycle in mice lacking miRNA-1-2. Cell *129*, 303–317.